Two-photon spectroscopy of MgO:Ni^{2+}

C. Campochiaro and D. S. McClure
Department of Chemistry, Princeton University, Princeton, New Jersey 08544

P. Rabinowitz and S. Dougal
Exxon Research and Engineering Company, Annandale, New Jersey 08801

(Received 21 May 1990)

We report polarized two-photon excitation spectra of the $^3A_2 \rightarrow {}^3T_2$, ^1E, and $a\ ^3T_1$ transitions of Ni^{2+}-doped MgO measured by detecting the $^3T_2 \rightarrow {}^3A_2$ infrared luminescence with a Ge photodiode. Two-photon excitation spectra of the $^3A_2 \rightarrow {}^1T_2$ and $b\ ^3T_1$ transitions were measured by monitoring the visible emission from the $^1T_2$ state. Hidden zero-phonon lines have been revealed as well as even-parity vibrational features. Additionally, the assignments of the well-known one-photon, odd-parity vibronic spectra have been confirmed by comparison with the two-photon spectra. The two-photon polarization ratios were measured for the $^3T_2(E)$ and $^3T_2(T_1)$ zero-phonon lines and an intensity calculation using only the d electrons was performed. The failure of this calculation demonstrated that the ligands significantly contribute to the overall two-photon intensity.

I. INTRODUCTION

The electronic spectrum of Ni^{2+} in MgO has been studied many times as it presents Ni^{2+} in a rigid, highly symmetrical site which should offer the minimum number of complications for spectral analysis. Works by Ferguson and co-workers,[1-4] Bird, Osborne, and Stephens,[5] Manson,[6-7] Moncorgé and Benyattou,[8] Payne,[9] and Silbey and co-workers[11,12] are especially notable and represent some of the different objectives of research on this and closely related systems.

Only the first ligand-field transition,

$$^3A_{2g}(T_{2g}) \rightarrow {}^3T_{2g}(A_{2g}, E_g, T_{1g}, T_{2g}) ,$$

is directly allowed in one-photon (OP) absorption by a magnetic dipole operator; the others are vibronically induced. However, spin-orbit components of all of the excited states are allowed via two-photon (TP) absorption. This means that the zero-phonon lines should be observable, and in view of the importance of this material we have recorded the two-photon spectrum. Many of the expected zero-phonon lines do in fact appear and make it possible to interpret this long-known spectrum in more detail, and several new questions are raised.

The electronic energy levels of MgO:Ni^{2+} are shown in Fig. 1. The Ni^{2+} ion substitutes for Mg^{2+} in the cubic lattice with O_h site symmetry. The ground state has $^3A_2$ symmetry. Three spin allowed transitions occur at approximately 9000 cm^{-1} ($^3T_2$), 15 000 cm^{-1} ($^3T_1$, denoted $a\ ^3T_1$), and 24 000 cm^{-1} ($^3T_1$, denoted $b\ ^3T_1$). In the strong-field limit, the only fully allowed two-photon transition is $^3A_2(e^2t^6) \rightarrow a\,^3T_1(e^3t^5)$. The $^3A_2 \rightarrow a\,^3T_1$ transition near 15 000 cm^{-1} contains the largest fraction of this component and should be the strongest of the two-photon transitions. Spin-orbit coupling splits each of these orbital triplets into four substates. The assignments of the various substates have been in question for many years, especially in the case of the $a\ ^3T_1$ manifold, which resides near and is strongly mixed with the ^1E state.[10]

Additionally, three singlet states are predicted by crystal-field theory to occur in the visible region of the spectrum at approximately 12 500 cm^{-1} (^1E), 21 000

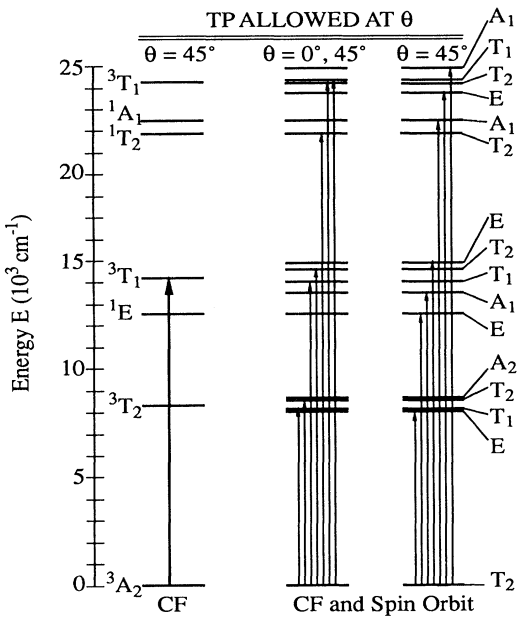

FIG. 1. Diagram of the energy levels and symmetry-based selection rules (Ref. 14) for a single-beam two-photon excitation of Ni^{2+} in an octahedral crystal field. In the absence of configuration mixing and spin-orbit coupling the only fully allowed transition from the ground state is $^3A_2(e^2t^6) \rightarrow a\,^3T_1(e^3t^5)$, and it would be polarized along a (110) axis ($\theta = 45°$), as indicated on the left side of the figure. This transition when mixed into the others gives the right side of the figure. Intraconfigurational components (e.g., $e^3t^5 \rightarrow e^3t^5$) give the selection rules in the center.

cm^{-1} ($^1T_2$), and 21 500 cm^{-1} ($^1A_1$). But, only the transitions to the ^1E and $^1T_2$ states have appreciable intensity due to spin-orbit mixing with the ^3T_1a and ^3T_1b states. These spin forbidden transitions appear as weak shoulders on the low-energy sides of the $^3A_2 \rightarrow {}^3T_1a$ and $^3A_2 \rightarrow {}^3T_1b$ transitions.

Three strong emissions have been assigned by Silbey and co-workers: $^3T_2(E) \rightarrow {}^3A_2$ in the near infrared, $^1T_2 \rightarrow {}^3T_2$ in the red, and $^1T_2 \rightarrow {}^3A_2$ in the green.[11,12] Short-lived $^1T_2 \rightarrow a\,{}^3T_1$ and ^1E emissions have been reported by Payne[9] in MgO:Ni^{2+} and Tonucci, Jacobsen, and Yen[13] for MgF_2:Ni^{2+}. Both the $^3T_2 \rightarrow {}^3A_2$ and the $^1T_2 \rightarrow {}^3A_2$ emissions were used to detect two-photon absorption.

Figure 1 shows the energy-level diagram of Ni^{2+} in a cubic field with energy-level spacings as they are found for MgO:Ni^{2+}. In two-photon spectroscopy of a cubic crystal there are three important polarizations[14] and Fig. 1 shows the two available with a single optical frequency (the only ones we used). With light propagating along one cube axis, the polarization can be along another or at 45° to it. The transitions $T_2 \rightarrow E$ and $T_2 \rightarrow A_1$ should be observed only at 45°. The $^3A_2$ ground state has an overall spin-orbit product symmetry T_2 so that E and A_1 states should appear at 45° and disappear at 0°. Transitions $T_2 \rightarrow T_2$, $T_2 \rightarrow T_1$ should appear with mixed polarization. In these cases, an intensity calculation must be performed to predict the relative magnitudes of the isotropic and polarized contributions to the overall intensity. The transitions $A_2 \rightarrow T_2$ are forbidden in a single-frequency experiment.

II. EXPERIMENT

A. Sample preparation

The MgO:Ni^{2+} crystal is the same one as was studied by Bird, Osborne, and Stephens.[5] The crystal is cleaved along the cube axes, so laser excitation was always normal to a (100) surface. The crystal was carefully mounted between indium-plated copper leaves to ensure good thermal contact and placed in an Air Products closed-cycle He refrigerator. Two gold-chromel thermocouples were used to monitor the temperature, one above and one below the crystal on the copper sample holder. The thermocouple closest to the refrigerator typically indicated 9 K and the other 13 K. The entrance and exit windows were tilted approximately 2°, to avoid etalon fringes.

B. Generation of polarized tunable ir radiation

All the spectra were obtained by excitation from a tunable, pulsed laser as depicted in Fig. 2. The tunable laser consisted of an injection seeded and doubled Quanta-Ray DCR-3 Nd:YAG laser pumping a Lambda-Physik FL2002 dye laser. The dye-laser output was channeled into a multipass Raman cell which is described in detail elsewhere.[15] One, two, or three Stokes shifts could be selected by varying the number of passes through the cell: first Stokes was obtained with one pass, second Stokes with three passes, third with fifteen. The third Stokes radiation was extracted from the lower-order Stokes fields by passing the light through a pair of Ge plates set at Brewster's angle. This served as a polarizer as well as a long-wavelength bandpass filter. The second Stokes radiation was similarly separated with an uncoated GaAs or Si plate. The incident pulse energy at the sample ranged from 100 μJ to 2 mJ and the power density approached 1 GW/cm^2 in the crystal.

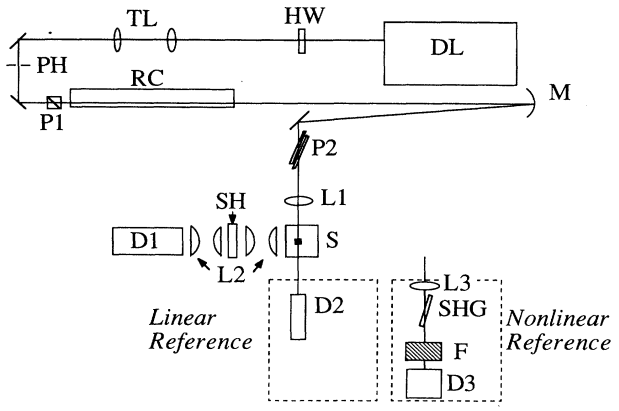

FIG. 2. Schematic of the two-photon (TP) IR excitation experiment. The output of an injection seeded Quanta Ray Nd:YAG pumped Lambda Physik dye laser (DL) is focused into a multipass Raman laser (RC) with a mode matching telescope (TL) to generate three 4155 cm^{-1} Stokes shifts. A half-wave plate (HW) is used to determine the direction of polarization. A Glan-Taylor prism (P1) placed before the RC is used to reduce the amplified spontaneous emission and any ellipticity in the beam, and a pinhole (PH) is used as a spatial filter. The third Stokes radiation is isolated with a double Ge Brewster window (P2), which also serves as a polarizer, and is focused into the cooled crystal (S) with a 4-m Au mirror (M1) and an achromatic 8″ lens (L1). The $^3T_{2g} \rightarrow {}^3A_{2g}$ emission is collected and focused onto a Uniblitz shutter (SH) and finally refocused onto a 77-K Ge photodiode (D1) with four $f/0.67$ lenses (L2). The reference was always taken after the exciting radiation passed through the crystal and was either linear or quadratic with respect to the intensity of the transmitted beam. The linear referencing scheme consisted only of a pyroelectric detector (D2). The nonlinear reference consisted of a piece of polycrystalline ZnSe at Brewster's angle, which acted as a second harmonic generator (SHG). The second harmonic radiation was collected with a 5-cm lens (L3) and filters (F) were used to separate the primary beam from the doubled light, which was detected with another 77-K Ge photodiode (D3).

The Raman laser shifts the fundamental frequency in increments of 4155 cm^{-1}, corresponding to vibrational transitions in H_2. Stimulated Raman scattering also occurs parasitically on rotational transitions producing multiple sidebands in each order at intervals of 587 cm^{-1} above and below the vibrational Stokes frequencies. In general these rotational sidebands are weak. A second group of even weaker sidebands may also appear at 354-cm^{-1} intervals. The latter arise from the small fraction of para-H_2 states occupied at ambient temperatures (25%), the former from the dominant (75%) ortho states. These weak parasitic oscillations are only important if they induce a one-photon transition, masking the much weaker two-photon transitions. Fortunately, they occur

at predictable frequencies, so we could confirm that this was not a problem in any of the spectra reported in this article.

The Stokes polarization was rotated by rotating the dye-laser radiation with a dielectric $\lambda/2$ plate. The dye-laser radiation was then passed through a Glan-Taylor polarizer before the Raman cell to eliminate any residual elliptical polarization, thereby minimizing the generation of rotational sidebands at multiples of 587 cm^{-1}. The desired polarization was ensured by placing an additional polarizer directly in front of the sample. The pair of Ge Brewster window plates acted as a filter and as a polarizer for the $^3T_2$ spectra while a Glan-Taylor prism had to be inserted for the ^1E and $a\,^3T_1$ spectra. The beam had to be realigned for each spectrum taken at a different polarization. Therefore, different portions of the crystal were sampled in different polarizations and with the possibility of generating laser-induced defects (see Sec. III A), quantitative comparisons of the spectra taken at different polarizations cannot be made.

C. Two-photon spectra of the $^3T_2$, ^1E, and $^3T_1 a$ states

The $^3T_2$ two-photon transition was excited with either third Stokes radiation from three different dyes: Rhodamine (Rh) 640/Rh 610($\sim$1:10), Rh 610, and Rh 610/Rh 6G($\sim$1:10) or with third Stokes radiation from Rh 640/Rh 610($\sim$1:10) and Rh 610, combined with second Stokes from LDS 765. The ^1E and $a\,^3T_1$ transitions were excited with the second Stokes shifts from three dyes: LDS 698/DCM($\sim$1:10), DCM, and DCM/Rh 640($\sim$1:10).

The fluorescence from the 8006-cm^{-1} zero-phonon line was collected and focused onto a Vincent Associates Uniblitz Shutter with a pair of $f/0.67$ aspheric crown glass lenses. Another lens pair reimaged the crystal 1:1 onto a North Coast 77-K Ge photodiode, which has a 1–2 ms response time, biased at -250 V. The shutter which screened laser scattered light from the detector was essential to the experiment. The timing sequence which also was critical is depicted in Fig. 3.

The Ge detector is sensitive to visible room light, mechanical vibration, and cosmic rays. Without the shutter, the Ge detector was easily saturated by scattered laser light when tuning through the $a\,^3T_1$ state ($\frac{1}{2}$ of 13 000–16 000 cm^{-1} is 6500–8000 cm^{-1}). The long time constant and recovery time from saturation of the detector made the use of the mechanical chopper mandatory.

Additionally, electrical noise at multiples of 60 Hz was a serious problem. To eliminate this noise, both signal and reference boxcars were gated twice during each optical pulse repetition cycle, first prior to the laser pulse, and then after the laser pulse but in the presence of the fluorescence emission. The time between these gates was maintained at a multiple of 16.667 ms, the 60-Hz period and the signal from the earlier gate subtracted from that of the later one.

The signal channel was further complicated by the fact that the detector could see the difference in blackbody radiation between the warm shutter and the cold crystal, causing a dip in the signal channel when the shutter opened. Our double-gate trick only worked when we double triggered the shutter as well and carefully synchronized the gates to the dips.

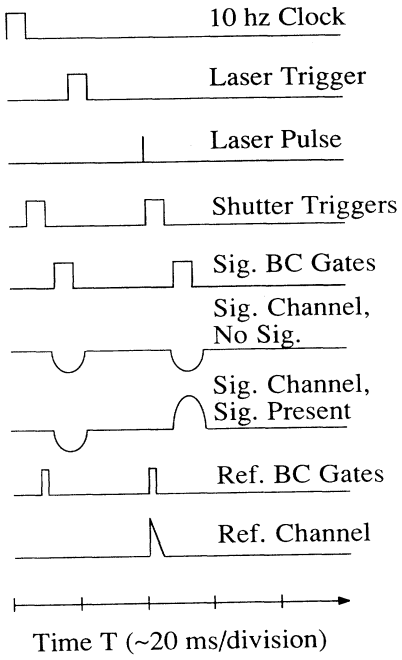

FIG. 3. Digital delays from a 10-Hz master clock provided triggers for the Nd:YAG laser, Uniblitz shutter, as well as signal and reference boxcars. The shutter and the boxcars had to be double triggered to eliminate 60-Hz noise, the measured signal taken as the difference before and after the laser fired. The bumps on the signal channel indicate how sensitive the Ge photodiode was: With no fluorescence present, the signal dropped when the shutters opened because the detector could no longer see black body radiation from the warm shutter leaves, only the 13-K sample.

The $^3T_2$ spectra were taken twice with different references as shown in Fig. 4: first with a pyroelectric detector placed just after the sample and again with a ZnSe nonlinear reference. Two-photon spectroscopy with multimode dye lasers has traditionally been difficult when the tuning range is spread over more than one dye. The temporal pulse width of the dye laser depends on the number of longitudinal modes oscillating; as threshold is approached on the edges of a dye tuning curve, fewer modes can oscillate, so the output pulses are shorter. When the integrated energy of each pulse is used as a reference, the spectrum can appear to rise at the juncture between two dyes. A nonlinear reference that depends on the square of the intensity of the pulses eliminates this effect.

An ideal second-harmonic generator (SHG) for referencing two-photon spectra would not have any absorbance near the region of interest, 2.0–1.0 μm, would not be phase matchable, and would have a large nonlinear index. ZnSe satisfies all these requirements. The experimental configuration used a ZnSe Brewster window behind the sample, followed by a glass collection lens, an 87-A Kodak Wrattan filter, an infrasil 10-mm cuvette

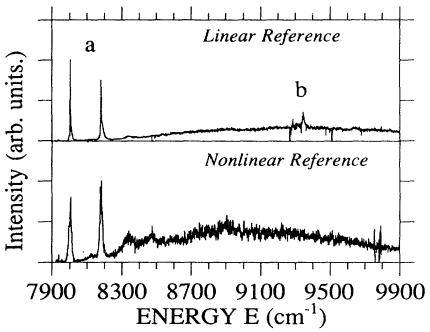

FIG. 4. Two-photon spectra of the $^3T_2$ state. The top spectrum was taken with a pyroelectric detector as the reference detector. The lower was taken with a Ge photodiode monitoring second-harmonic generation in ZnSe, and should represent a quadratic response to the input intensity as in two-photon absorption. (a) denotes a change in the relative intensity of the $^3T_2(E)$ and $^3T_2(T_1)$ zero-phonon lines and (b) marks an artifact that occurs on the edges of dye tuning curves. Note that the differences in the overall shape, zero-phonon linewidths, and noise levels are not due to the nonlinear reference, but probably are due to optically induced defects in the crystal.

filled with a mixture of H_2O and D_2O, and a Judson Infrared 77-K Ge detector. The Brewster window was necessary to eliminate the reflection of second-harmonic light from the back surface of the ZnSe which excited the MgO:Ni^{2+} in a single-photon process and saturated the North Coast Ge detector.

The linearly referenced spectra were simply the fluorescence signal divided by the square of a pyroelectric signal. The nonlinearly referenced spectra were the fluorescence signal divided by the second-harmonic signal times correction factors for the filter transmission curves, the Ge detector response, and the coherence length in the ZnSe. We assumed that $\chi^{(2)}$ of ZnSe remained constant since the experimental wavelengths were far from any resonance.

D. One-photon spectra of the $^3T_2$, ^1E, and $^3T_1 a$ states

Although many authors have published the absorption spectrum of the $^3T_2$ state,[5,8,16–18] none have published a low-temperature spectrum with the two prominent zero-phonon lines on scale clearly enough to measure the relative intensity of the origins to the sideband. Additionally, the ^1E state has an unusual shape and we hoped that a detailed laser excitation spectrum would reveal fine structure.

The one-photon excitation spectra of the $^3T_2$ state were obtained from second Stokes and Rh 640/Rh 610(~1:10), Rh 610, and Rh 610/Rh 6G and first Stokes from LDS 722. The ^1E state was excited directly with LDS 800. The excitation light was not focused in the crystal. A Judson Infrared 77-K Ge detector with a Si filter was used in place of the more sensitive North Coast detector and referenced against a pyroelectric detector placed after the crystal.

Using the transmitted light as the reference was convenient because changes in incident intensity due to any optical element before the sample that absorbed light or generated an etalon fringe pattern were ratioed out. The excitation spectra were corrected for sample absorption.

E. Two-photon spectra of the $^1T_2$ and $^3T_1 b$ states

These spectra were obtained in the same way as the linearly referenced lower-energy transitions except that the green emission from the $^1T_2$ state was monitored. An EMI 9558 QB photomulplier tube fitted with a broadband blue-green interference filter replaced the Ge photodiode. The shutter was kept open.

III. RESULTS

A. $^3T_2$ spectra

Figure 5 shows the one- and two-photon excitation spectra of the $^3T_2$ multiplet. The $^3T_2$ state is split by spin-orbit coupling into four substates which are predicted to lie in order of increasing energy: E, T_1, T_2, and A_2. The two multiplet components already known from the one-photon spectrum and assigned with the help of spin-orbit splitting calculations[19] are E_g (8006 cm^{-1}) and T_{1g} (8183 cm^{-1}). Figure 5 shows that they have the expected two-photon polarizations, experimentally confirming their assignments. The T_{2g} component may not have been observed. The A_2 component, which is forbidden in the two-photon spectrum, was not observed.

Experimental problems had to be faced when dealing with this spectrum. Figure 4 compares the spectra using a linear and a nonlinear reference. The spurious peak with the linear reference is due to laser pulse shape effects at the ends of dye ranges. The phonon sidebands have a different shape for the two experiments; presumably the nonlinear reference is more likely to be correct. On the other hand, after many two-photon runs with incident radiation of about 1 GW/cm^2, this spectral region looks different from earlier runs. We suspect some type of damage, although no macroscopic flaws are visible through a microscope.

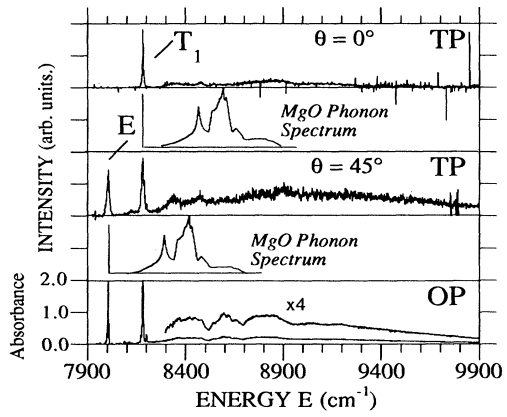

FIG. 5. One- and two-photon spectra of the $^3T_2$ state plotted with the phonon spectrum of MgO at the E_g and T_{2g} origins. The two-photon spectra were taken with a nonlinear reference.

The phonon sidebands in the one- and two-photon spectra look different as seen in Fig. 5. This is somewhat surprising as the $^3A_2 \rightarrow {}^3T_2$ transition is reported to be purely magnetic dipole.[20,21] At 0°, only one multiplet component contributes a sideband and the spectrum is simpler than either the 45° spectrum or the one-photon spectrum. Because of the issue of potential damage, it is hard to say much more.

Figure 5 also shows the spectra with the density-of-states profiles superposed on the two origins.[22] One sees a reasonable correlation between the main phonon density peak of 400 cm^{-1}, and the sideband maxima of the two origins. This same correlation will be made in other spectra and can be used to make reasonable guesses as to the energies of zero-phonon lines. It is tempting to assign the third broadband to the T_2 component which would place the energy of the zero-phonon line between 8400 and 8550 cm^{-1}. This agrees fairly well with the two independent calculations.

B. $^1T_2$ spectra

The zero-phonon line of the $^3A_2 \rightarrow {}^1T_2$ transition was observed by Moncorgé and Benyattou[8] in a two-photon excited-state excitation experiment using the green luminescence from the upper state for detection. Our data, shown in Fig. 6 along with Bird, Osborne, and Stephens' one-photon spectrum, corroborate their zero-phonon line. The vibronic sidebands in our two-photon spectrum differ from those observed by Moncorgé and Benyattou because the excited-state excitation experiment is one-photon excitation from a higher excited state so odd-parity vibrational features are allowed. Figure 6 also shows the analysis of the one-photon spectrum using the superposition of the density of states of MgO positioned with the help of the two-photon spectrum. The second main feature of the one-photon spectrum is clearly coincident with the 400-cm^{-1} lattice mode; the first feature at 180 cm^{-1} does not correspond to any feature in the density of states, and therefore must be a local mode. This assignment was made theoretically by Sangster and McCombie,[22] but Fig. 6 confirms it experimentally.

The 280-cm^{-1} peak in the density of states consists of longitudinal acoustic (LA) phonons[6] and does not appear in the one-photon spectrum. The latter is induced by odd-parity t_{1u} modes which appear as transverse optical phonons at the zone edge near 400 cm^{-1}. The two-photon spectrum, however, shows a broadband from 100 to 300 cm^{-1} which may have contributions from these LA modes. The other peaks in the two-photon spectrum can be explained as combinations of the first two peaks with 400 cm^{-1} phonons. The polarization of the zero-phonon line agrees with its assignment to the $^1T_{2g}$ state, and not to the nearby $^1A_{1g}$ state or the related ^1E_g state.

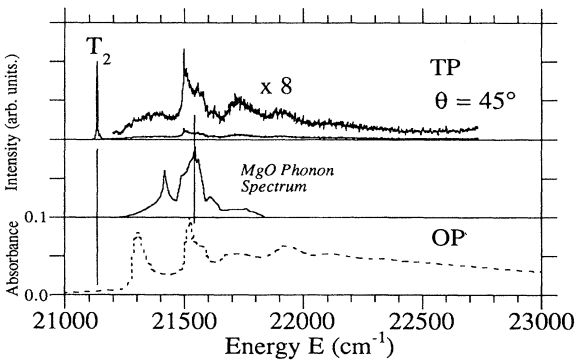

FIG. 6. Bird, Osborne, and Stephens' one-photon (Ref. 5) and our two-photon spectra of the $^1T_2$ state are plotted along with the photon density of states for MgO (Ref. 22).

C. ^1E_g spectra

The ^1E_g state was studied in an early paper by Jorgensen.[23] His method was to vary the crystal field on the Ni^{2+} ion by changing the ligands. In this way, the weak spin-forbidden $^3A_2 \rightarrow {}^1E$ transition could be traced from weak to strong fields even though it is strongly perturbed by the $^3T_{1g}(E)$ state in a wide range of intermediate fields. This perturbation was well illustrated by comparing the data to the energies given by the crystal-field matrix. In the case of MgO:Ni^{2+}, a full crystal-field calculation places a state which is largely ^1E at 12 500 cm^{-1}. In this spectral region there is a broad weak band from 12 600 to 13 600 cm^{-1} in the one-photon spectrum, as shown in Fig. 7.

The two-photon spectrum begins at 12 500 cm^{-1} in the 45° polarization, and is hardly observable in the 0° polarization, as seen in Fig. 7. The sharp band at 13 511 cm^{-1} is assigned as the first spin-orbit component of $^3T_{1g}$. The polarization of the broadband is in agreement with its assignment to $^3A_2 \rightarrow {}^1E$. There is no structure that we can identify with certainty, but it is clear that the one-photon spectrum has vibrational features corresponding to those of the $^1T_{2g}$ state though broadened. Thus, the weak

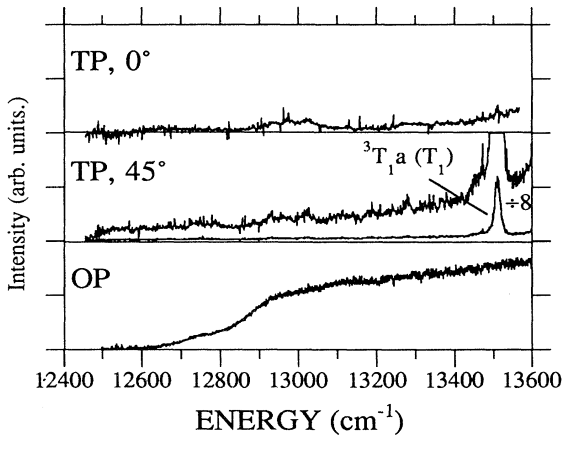

FIG. 7. The one-photon and polarized two-photon spectra of the ^1E state are plotted against the transition energy. This is uncorrected data; the sharp spikes are reportedly due to cosmic rays. The features at 13 000 cm^{-1} are visible in both the 0° and 45° spectra, are unassigned, and are probably due to a different defect center in the crystal. Note that the origin of the $a^3T_1(T_1)$ state on the high-energy side of the spectra is strongly polarized, as predicted by Bader and Gold (Ref. 14).

shoulder near 12 700 cm^{-1} in the one-photon spectrum corresponds to the addition of the 180-cm^{-1} local mode to the origin at 12 500 cm^{-1}, and the strong shoulder at 12 900 cm^{-1} corresponds to the addition of the 400-cm^{-1} band mode to the origin. This analysis could not have been made with confidence without knowledge of the origin energy given by the two-photon spectrum. The 12 500-cm^{-1} origin has a bandwidth of about 100 cm^{-1}.

D. $b\,^3T_{1g}$ spectra

As shown in Fig. 8 only one sharp multiplet component of $b\,^3T_{1g}$ appears in the two-photon spectrum and its 45° polarization is in agreement with an assignment to an E_g state. When the MgO phonon spectrum is superposed on the one-photon spectrum, using the E_g origin found in the two-photon spectrum, we see a result similar to those found for the $^1T_2$ and ^1E states. The second band coincides with the 400-cm^{-1} peak of the phonon spectrum while the first does not coincide with any feature of the phonon spectrum. It is therefore assigned as a local mode, and its frequency of 180 cm^{-1} is the same as was found for the $^1T_2$ and ^1E states.

The other feature in the two-photon spectrum is a weak broadband at 240 cm^{-1} polarized at 45°. The $^3A_{2g} \rightarrow b\,^3T_{1g}(A_1)$ transition should be polarized in this way but ought to appear about 500 cm^{-1} above the first multiplet component. The 280-cm^{-1} peak in the density of states could appear as a sideband to the first component, and would have the correct polarization, but would be shifted. Neither assignment is easy to accept. The rising background of this spectrum appears to be unpolarized in the two-photon spectrum and it also appears in the one-photon spectrum.[5]

E. The $a\,^3T_{1g}$ spectra

Figure 7, referred to previously, showed a two-photon line at 13 511 cm^{-1} polarized at 45°. It's width is 17 cm^{-1} at 13 K. Because of its position and polarization, it appears to be a component of the $a\,^3T_1$ multiplet. Whether the feature should be assigned to the A_1 or T_1 spin-orbit component is discussed in Sec. IV.

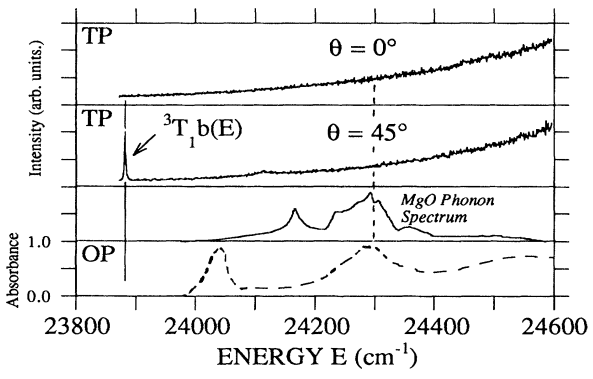

FIG. 8. Bird, Osborne, and Stephens' one-photon spectrum (Ref. 5) and our polarized two-photon spectra of the b^3T_1 state are plotted with the phonon density of states of MgO (Ref. 22).

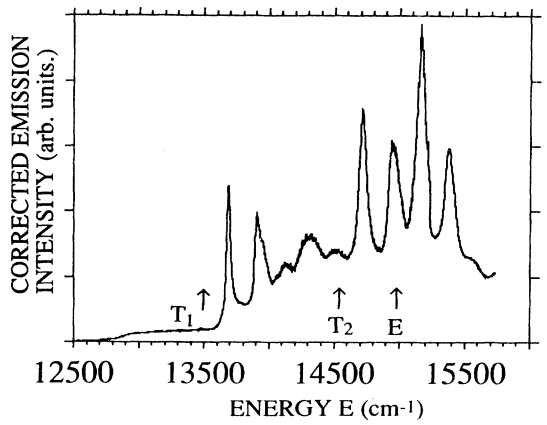

FIG. 9. The one-photon excitation spectrum of the $a\,^3T_1$ multiplet is shown along with arrows marking the location of three zero-phonon lines, currently assigned as the T_1, T_2, and E states.

Figure 9 shows the one-photon excitation spectrum of the $a\,^3T_1$ multiplet (including ^1E). The first pair of bands, at 13 685 and 13 930 cm^{-1} may correspond to phonon sidebands of the lowest spin-orbit component of the multiplet. As in Fig. 7, if we position the phonon density spectrum of MgO with its zero on the 13 511-cm^{-1} line, we see that the 13 930-cm^{-1} band coincides with the 400-cm^{-1} peak of the phonon density of states, while the 13 685-cm^{-1} band falls in a featureless region of acoustic lattice modes (Fig. 10). This is the same behavior as has already been observed for the $^3T_2$, $^1T_2$, $b\,^3T_1$, and ^1E, and it supports the identification of the 13 511-cm^{-1} line as a zero-phonon line of a $^3T_1$.

The photons which excite the observed component have 6750 cm^{-1}, which is about 1250 cm^{-1} below the first one-photon resonance at 8006 cm^{-1}. When we scanned above 6250 cm^{-1}, other lines and a rising background were observed, the beginnings of which are shown in Fig. 10. The fluorescence detector is sensitive to radiation from 7900 to 5800 cm^{-1}. The additional lines and background also appeared in an experiment using the same pulse energy but with an unfocused beam. In addition they are unpolarized. It must be concluded that these are one-photon excitation features. The rising background behaves approximately as $(8006\text{-}\bar{\nu})^2$ where $\bar{\nu}$ is the laser frequency in cm^{-1}.

It is possible that the sharp features are due to Ni^{2+} pairs or other Ni^{2+} containing defects which would have a fluorescence spectrum and lifetime similar to those of the cubic Ni^{2+} single ions. They are not due to single Fe^{2+} or Co^{2+} impurities, which have well-known spectra in MgO.[24,25] Another crystal from a different source[26] showed some but not all of the same lines, and also the rising background. The onset of these features is seen to the blue of the $a\,^3T_1(A_1)$ zero-phonon line in Fig. 10 as a slightly rising background and two weak resonances at approximately 13 900 cm^{-1}.

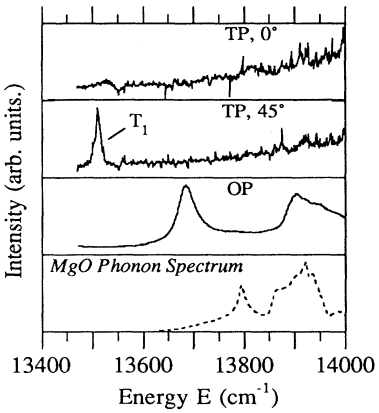

FIG. 10. One- and two-photon spectra of the $a\,^3T_1(T_1)$ state are shown along with the phonon density of states for MgO:Ni^{2+}. Note the rising background in the TP spectra. This is not due to Ni^{2+} in a cubic site and is probably the result of one-photon emission of another defect center in MgO. The $a\,^3T_1(T_1)$ state does not appear to have a vibrational sideband since that would also be strongly polarized.

IV. DISCUSSION

The two-photon spectra do not provide all of the expected zero-phonon lines. Table I lists the ones observed in these experiments. The two $^3T_2$ components have been reported before,[5,8] and Payne[9] has reported the origin observed at 13 511 cm^{-1}. Moncorgé and Benyattou[8] reported the zero-phonon lines of the $^1T_2$ state from excited-state excitation experiments and the zero-phonon lines of the $b\,^3T_1$ state from two-photon excitation, which we have also done. Our interpretation of the ^1E two-photon spectrum provides another zero-phonon "line," much broadened.

A. Assignments

The key to making the assignments is to realize the correlation between the one- and two-photon spectra. Figure 6 illustrates this quite clearly, as the $^1T_2$ state only contains one triply degenerate state. The zero-phonon line is observed in the two-photon spectrum at 21 134 cm^{-1} and the most prominent phonon peak is centered at approximately 400 cm^{-1} higher in energy. With the phonon density of states superimposed on the spectrum and originating at the zero-phonon line, it is clear that the major feature of the phonon sideband and the phonon density of states coincide. In addition, the one-photon spectrum at the bottom of the figure also contains a prominent feature at 400 cm^{-1} above the zero-phonon line. This is not surprising since Manson's 1971 paper[6] showed that all the symmetry-projected phonon sidebands have maxima at ~400 cm^{-1}. In other words, the two-photon spectrum, which should include contributions from t_{2g}, e_g, and a_{1g}, should display the prominent phonon sideband at the same energy as the one-photon spectrum, which includes contributions from the t_{1u} and t_{2u} modes. The second prominent feature in the one-photon spectrum at approximately 180 cm^{-1} from the origin and originally analyzed by Manson[6] is a local

TABLE I. The experimentally measured zero-phonon (ZPL) energies are listed in cm^{-1} along with the energies of the Franck-Condon maxima (FC center) used to fit the spectrum with a crystal-field calculation based on the matrix elements in Ref. 19 with the parameters $10Dq = 8889$ cm^{-1}, $B = 832$ cm^{-1}, $C = 3870$ cm^{-1}, and $\zeta = 325$ cm^{-1} (the same value used for the free ion). The results are listed and compared to the experimental energies suggested by Moncorgé and Benyattou (Ref. 8) and the calculated results from Bird, Osborne, and Stephens (Ref. 5). Note that Moncorgé and Benyattou also estimated many of the energies and these are listed in parentheses.

	Experimental and calculated energies for the visible spectrum of MgO:Ni^{2+}				
	Experimentally derived energies			Calculated energies (spacings)	
	This work		Ref. 8	This work	Ref. 5
Assignments	ZPL	FC centers	ZPL	FC centers	FC centers
$^3T_2(E)$	8 006(0)	8 605	8 002	8 607(0)	8 512(0)
$^3T_2(T_1)$	8 183(178)	8 783	8 180	8 785(178)	8 650(138)
$^3T_2(T_2)$			(8 422)	9 183(576)	8 978(466)
$^3T_2(A_2)$			(8 842)	9 350(743)	9 118(606)
^1E	12 500±30	13 650	(~13 000)	13 649	13 346
$a\,^3T_1(A_1)$			(13 000±100)	13 838(0)	13 780(0)
$a\,^3T_1(T_1)$	13 511(0)	14 111	(13 500±100)	14 339(501)	14 196(416)
$a\,^3T_1(T_2)$	14 550(1039)	15 150	(14 300±100)	15 275(1437)	14 842(1062)
$a\,^3T_1(E)$	14 990(1479)	15 580	(14 750±100)	15 650(1812)	15 225(1445)
$^1T_2$	21 134	21 734	21 100	22 198	21 790
$^1A_1$				22 754	22 300
$b\,^3T_1(E)$	23 897(0)	24 587	23 895(0)	24 587(0)	24 705(0)
$b\,^3T_1(T_2)$			24 040	24 840(253)	24 924(219)
$b\,^3T_1(T_1)$			(24 200±100)	24 951(364)	25 035(330)
$b\,^3T_1(A_1)$			(24 400±100)	25 136(549)	25 204(499)

mode. The absence of any feature in the phonon density of states at 180 cm^{-1} confirms this local-mode assignment. The combination of local and band mode in the one-photon spectra act as markers for the location of zero-phonon lines.

Figure 8 of the $b\,^3T_1$ state is similar to Fig. 6. The $b\,^3T_1(E)$ zero-phonon line is observed in the two-photon spectrum and it supports the assignment of the two phonon bands seen in the one-photon spectrum. The spectrum is puzzling, however, since one would expect to see the T_1 and T_2 components as well. The one-photon spectrum, taken from Ref. 5, also fails to show strong evidence of the higher-energy multiplets. The only prominent features are the two bands that must be associated with the $b\,^3T_1(E)$ state. The one-photon intensity at higher energy is probably due to the other components, but unlike the $a\,^3T_1$ state, their structure is obscured. A possible explanation is that the higher-energy features are broadened by their proximity to a charge-transfer transition. The rising background seen in both the one-[5] and two-photon spectra (note Fig. 8) suggests this explanation.

Moncorgé and Benyattou's excited-state absorption experiments led to an assignment of the two lowest multiplet components of $b\,^3T_1$.[8] They identified the two-photon line at 23 895 cm^{-1} at 80 K as the lowest, or E, component. We observe this line, at 23 897 cm^{-1} at 13 K, and our observation that the line is polarized at 45° in two-photon excitation supports their assignment. The excited-state absorption experiment gave a value of 149 cm^{-1} for the $E(T_2)$-$E(E)$ interval, putting $b\,^3T_1(T_2)$ at 24 044 cm^{-1}, but no such feature is discernible in our spectra even though the two-photon selections rules permit this transition.

The $^3T_2$ state can be analyzed in the same way, and this is shown in Fig. 5. The two-photon spectrum at 45° is similar to the one-photon spectrum, since this is a magnetic dipole transition.[5] If phonon density-of-states curves are placed at the $^3T_2(E)$ and $^3T_2(T_1)$ origins, shown in the figure, the first two maxima in the phonon sideband clearly correspond to the maximum density of states from each origin. Additionally, most of the detailed structure in the density-of-states function is reproduced in the one-photon magnetic dipole spectrum. There is no clear evidence for the $^3T_2(T_2)$ or the $^3T_2(A_2)$ origins, although Bird, Osborne, and Stephens' magnetic dipole analysis predicts considerable intensity in the $^3T_2(T_2)$ state.[5] It is reasonable to assume that the $^3T_2(T_2)$ origin lies well in the phonon sidebands of the $^3T_2(E)$ and $^3T_2(T_1)$ states and could be broadened due to rapid decay into those states.

Evidence for the position of three multiplet components of the $a\,^3T_1$ state is found in the one-photon spectrum, as has been pointed out before.[5,8] The three pairs of bands in this spectrum must correspond to sidebands of three multiplet components of which one has been observed by us in two-photon excitation and tentatively assigned as T_1, in agreement with Ref. 8. As already discussed above, fitting the phonon spectrum of MgO to this origin shows that the first member of the pair is the 180-cm^{-1} local mode and the second is the approximately 400-cm^{-1} band mode. The same fitting gives two other origins at 14 550 and 14 990 cm^{-1}. When the appropriate $S\hbar\omega$ is added, these fall close to the calculated values, which will be presented in Sec. V C.

Figure 9 shows the one-photon spectrum of the $a\,^3T_1$ state with the three "known" multiplet component origins marked by vertical arrows. Figure 9 also shows that the local-mode intensity is greater than that of the band mode for three of the multiplet components. Possibly, therefore, the broad strong band at 14 300 cm^{-1} is the local mode associated with the missing multiplet component; if so the zero-phonon line would occur at 14 120 cm^{-1} which is a reasonable value. This conjecture is difficult to verify, however, because there might be multiphonon transitions built on the 13 511 cm^{-1} origin which would contribute to the spectrum in the region between 14 000 and 14 600 cm^{-1}.

The beginning of the 45° two-photon spectrum of the ^1E state shows that the zero-phonon line must be broadened to about 100 cm^{-1} width at half maximum. That this is the true origin of the state is supported by Payne's recent paper[9] showing that the onset of the infrared $^1T_2 \rightarrow {}^1E$ transition coincides with the onset of our two-photon spectrum. Since the $^1T_2 \rightarrow {}^1E$ is magnetic dipole allowed, it is expected that the origin would appear.

B. Franck-Condon factor analysis

Since several multiplet components do not appear directly in the spectra, a full crystal-field calculation using the matrices of Liehr and Ballhausen[19] was done to see where they should occur and as an aid to further interpretation of the spectra. In order to provide data with which to fit a theoretical calculation we must add $S\hbar\omega$ to the zero-phonon lines. Here S is the average Huang-Rhys factor and $\hbar\omega$ is an average configuration-coordinate energy. Since the major frequencies of the MgO lattice cluster around 400 cm^{-1}, this can be taken as the value for $\hbar\omega$.

The average Huang-Rhys factor S for all modes can be found from

$$\frac{I_0}{I_0+\sum_i I_i} = e^{-S} . \tag{1}$$

A somewhat inaccurate value can be obtained for the $^1T_2$ state from the data of Fig. 6: the area under the origin, I_0, is obtainable from the linewidth since the spectral resolution was not laser limited; and the area of the broad band, $\sum_i I_i$, can be obtained if the signal is large enough relative to the noise and background from extraneous sources. Thus, a rough value of $S = \ln 7.7 = 2.0$ is obtained for $^1T_2$. The small value is in part the effect of the very stiff lattice.

The S factor for the E component of $^3T_2$ is obtainable from the 0° polarization shown in Fig. 5 since the T_1 component does not contribute and the T_2 component is weak. The noise level is quite high but we estimate that

S_{T_1} is about the same as the Huang-Rhys factor for the $^1T_2$ state, about 1.9. By subtracting the 0° spectrum from the 45° spectrum with the proper scaling factor, we should be able to derive the S factor for the E component, assuming the intensity of the T_2 component is small; but the signal-to-noise ratio is too small. However, although the uncertainty is large, there is no indication that S_E is very different from the others.

The overall band shape of the $a\ ^3T_1$ multiplet was not obtained inTP excitation for reasons discussed earlier, but it is clear that the S factor of the observed component must be small since there is so little background for 500 cm^{-1} above it.

These results lead us to believe that S factors for the observed states of Ni^{2+} are small except for the ^1E state for which the zero-phonon line is not clearly resolved. Thus, about 600 cm^{-1} should be added to the zero-phonon line energy to provide a target for the crystal-field calculation. The average S factor for the ^1E state can be estimated to be about 3.

These conclusions about the S factors could have been reached from an examination of the one-photon data, although with less assurance. Most of the sideband structure in the one-photon spectrum relates to the intensity producing mechanism, but it is clear that there are no strong additions of symmetric modes to the t_{1u} vibrational false origins.

C. Crystal-field calculation

The results from the crystal-field calculation[19] are shown in Table I. The table lists the data measured in this report along with the data from Moncorgé and Benyattou's paper[8] and the results of another ligand field calculation by Bird, Osborne, and Stephens.[5] Our calculation was used to fit the Franck-Condon maxima of the states. The calculated energies are listed with a relative zero-phonon line energy in parentheses so that the structure of each multiplet could be examined. The $^3T_2$ experimental spacing is only known for the first two, 0 and 178 cm^{-1}. The calculation successfully predicted this spacing and predicted that the $^3T_2(T_2)$ and $^3T_2(A_2)$ states lie at 576 and 743 cm^{-1} from the $^3T_2(E)$ state. The ^1E state is more difficult to predict since the experimental spectrum does not contain any structure; however, the calculation fit the estimated Franck-Condon center to within 150 cm^{-1}. The absolute energy of the $a\ ^3T_1$ multiplet was predicted to fall in the correct region, but the relative spacing between the components is poorly fit: the data suggest the pattern is either $A_1(?)$, T_1 (0 cm^{-1} = 13 511 cm^{-1}), $T_2(T_1+1039\ cm^{-1})$, $E(T_1+1479\ cm^{-1})$ assuming the 13 511-cm^{-1} feature is the T_1 component. Our calculation gives the relative energies of A_1, T_1, T_2, and E as 0, 501, 1437, and 1812 cm^{-1}, alternatively written as -501, 0, 936, and 1311 cm^{-1} relative to the T_1 origin. Assigning the observed feature as the T_1 origin implies that the A_1 component lies near 13 000 cm^{-1}, but no polarized feature is observed there in TP excitation. The $^1T_2$ and $b\ ^3T_1(E)$ energies agree fairly well with experiment, although the data on the $b\ ^3T_1$ multiplet splitting is very incomplete.

D. Calculation of relative two-photon intensities and polarization ratios

Since the major configuration component of the $^3A_2$ ground state is t^6e^2, the only strong one-electron transitions are to the states having t^5e^3 components and are polarized at 45° (see Fig. 1). However, the electron-electron and spin-orbit perturbations mix the configurations. The resulting minor configuration components introduce other polarizations. In order to estimate these polarizations a calculation of the composition of the states was made, as discussed in the previous section. This was a standard crystal-field calculation, and the results are by no means certain to be adequate. In addition, however, there were standard approximations made in the two-photon intensity calculations which must also be questioned[27–29] and these will be addressed in this section.

The intensity of a single-beam two-photon transition is proportional to an expression of the form

$$I_{\mathrm{TP}} \propto \sum_i \left| \frac{\langle f|\mathbf{e}\cdot\mathbf{r}|i\rangle\langle i|\mathbf{e}\cdot\mathbf{r}|g\rangle}{E_i - E_g - h\nu} \right|^2 . \tag{2}$$

as described in Bader and Gold.[14] The two-photon operator can be divided into several symmetry adapted operators containing the irreducible representations of the direct product

$$T_{1u} \otimes T_{1u} = A_{1g} + E_g + T_{1g} + T_{2g} ,$$

although in the case of a single-beam experiment the T_{1g} operator will always be zero.[30] These are listed in Table II.

The first part of each expression in Table II is a one-electron operator, while the second is a photon operator.[31] l, m, and n represent direction cosines along x, y, z, as in Ref. 14. Since the photon operator does not operate on the electronic wave functions, it can be handled after the electronic matrix elements have been calculated. If the assumption that the excitation beam will always propagate along z is included the expressions in Table II reduce to

$$\begin{aligned}
\hat{O}_{a1}^{A_{1g}} &= \frac{1}{\sqrt{3}}(x^2+y^2+z^2)\frac{1}{\sqrt{3}}(l^2+m^2) , \\
\hat{O}_{\theta}^{E_g} &= \frac{1}{\sqrt{6}}(x^2+y^2-2z^2)\frac{1}{\sqrt{6}}(l^2+m^2) , \\
\hat{O}_{\varepsilon}^{E_g} &= \frac{1}{\sqrt{2}}(-x^2+y^2)\frac{1}{\sqrt{2}}(-l^2+m^2) ,
\end{aligned} \tag{3}$$

and

$$\hat{O}_{\zeta}^{T_{2g}} = -\sqrt{2}xy - \sqrt{2}lm .$$

These operators now contain the polarization dependence of the two-photon transition moment and Eq. (2) can be rewritten as

$$I_{\mathrm{TP}} \propto \sum_{\gamma} \left| \frac{\langle f|\hat{O}_{\gamma}^{\Gamma}|g\rangle}{\Delta E_{gi} - h\nu} \right|^2 . \tag{4}$$

With the operators written in real form, it is straightforward to decompose the eight-electron or two-hole

TABLE II. Single-color two-photon operators for the octahedral point group. The first part of each expression, $f(x,y,z)$, is a one-electron operator and the second, $f(l,m,n)$, is a photon operator. l, m, and n are direction cosines along (x,y,z) and contain the two-photon polarization. They are identical to those in Ref. 14 except that they have been written in symmetry-adapted form.

Symmetry-adapted single-beam two-photon operators for the O_h point group
$\hat{O}^{A_{1g}}_{a1} = \frac{1}{\sqrt{3}}(x^2+y^2+z^2)\frac{1}{\sqrt{3}}(l^2+m^2+n^2)$
$\hat{O}^{E_g}_{\theta} = \frac{1}{\sqrt{6}}(x^2+y^2-2z^2)\frac{1}{\sqrt{6}}(l^2+m^2+2n^2)$
$\hat{O}^{E_g}_{\varepsilon} = \frac{1}{\sqrt{2}}(-x^2+y^2)\frac{1}{\sqrt{2}}(-l^2+m^2)$
$\hat{O}^{T_{2g}}_{\xi} = -\sqrt{2}yz-\sqrt{2}mn)$
$\hat{O}^{T_{2g}}_{\eta} = -\sqrt{2}xz-\sqrt{2}\ln$
$\hat{O}^{T_{2g}}_{\zeta} = -\sqrt{2}xy-\sqrt{2}lm$

wave functions into products of one-hole t_{2g} and e_g wave functions using Table A20 in Griffith.[32] For example, ${}^3A_2(T_2)\xi=(1/\sqrt{2})(\theta\varepsilon-\varepsilon\theta)x_s$ where x_s is the x component of the spin part of the wave function. Since the two-photon operator is spin independent, it is not necessary to consider explicitly the spin part of the wave functions.

As described previously, the full crystal-field matrices of Liehr and Ballhausen[19] were used to fit the experimentally measured spectrum and exact eigenvectors. The major contributions to the eigenvectors are presented in Table III. The calculation was simplified by the fact that the ground-state wave function is fairly pure:

$$ {}^3A_2 = 0.99\,{}^3A_2(e^2)+0.10\,{}^3T_2(et)+0.03\,{}^1T_2(et)\ . $$

The small ${}^1T_2$ contribution was only considered in transitions to the singlet states. ΔE was taken as 4.0 eV from Powell and Spicer's diffuse reflection study[33] of NiO showing the onset of charge-transfer structure at that energy.

A one-photon magnetic dipole intensity calculation of the one-photon ${}^3A_2 \rightarrow {}^3T_2$ transition was also undertaken to check our wave functions against those of Ref. 5. The values were quite similar: we calculated the relative intensities for the E, T_1, T_2, and A_2 components as 0.18, 0.33, 0.38, and 0.11 compared to their values of 0.24, 0.36, 0.30, and 0.09. Note that we could not reproduce their results exactly with the crystal-field calculation because they used a weak-field approach including a Trees correction.[34]

The results of the two-photon relative intensity calculation and a comparison with the ${}^3T_2$ polarization data is presented in Table IV. All of the features that were experimentally observed in this study are completely polarized by symmetry except the T_1 and T_2 components of the ${}^3T_2$ multiplet and the ${}^1T_2$ state, hence these examples provide our only experimentally measured polarization ratios. The ${}^3T_2$ spectra provide an opportunity to measure the intensity ratio between the E and T_1 components at 45°. The polarization ratio of the T_1 component was measured by scaling the spectra to fit the $\sin^2 2\theta$ dependence of the E component, since the experiment was not designed to measure polarization ratios quantitatively. Figure 11 shows the scaled intensity changes of the E and T_1 components at four different polarizations. The polar-

TABLE III. Ni^{2+} crystal-field wave functions calculated using the matrices of Ref. 19. Only the majority components of each state are listed. The parameters used were $10Dq = 8889\ cm^{-1}$, $B = 832\ cm^{-1}$, $C = 3870\ cm^{-1}$, and $\zeta = 325\ cm^{-1}$.

Ni^{2+} wave functions arising from the d electrons in a cubic field
${}^3A_2(T_2) = 0.99\,{}^3A_2(e^2)+0.10\,{}^3T_2(et)+0.03\,{}^1T_2(et)$
${}^3T_2(E) = 0.98\,{}^3T_2(et)-0.09\,{}^3T_1(et)-0.11\,{}^3T_1(t^2)$
${}^3T_2(T_1) = 0.99\,{}^3T_2(et)+0.07\,{}^3T_1(et)+0.08\,{}^3T_1(t^2)$
${}^3T_2(T_2) = -0.10\,{}^3A_2(e^2)+0.99\,{}^3T_2(et)-0.07\,{}^3T_1(t_2)$
${}^3T_2(A_2) = 1.0\,{}^3T_2(et)$
${}^1E(E) = 0.42\,{}^3T_1(et)+0.29\,{}^3T_1(t^2)+0.84\,{}^1E(e^2)-0.15\,{}^1E(t^2)$
$a\,{}^3T_1(A_1) = +0.72\,{}^3T_1(et)+0.69\,{}^3T_1(t^2)$
$a\,{}^3T_1(T_1) = -0.11\,{}^3T_2(et)+0.73\,{}^3T_1(et)+0.67\,{}^3T_1(t^2)$
$a\,{}^3T_1(T_2) = 0.76\,{}^3T_1(et)-0.65\,{}^3T_1(t^2)$
$a\,{}^3T_1(E) = 0.18\,{}^3T_2(et)+0.64\,{}^3T_1(et)+0.55\,{}^3T_1(t^2)-0.50\,{}^1E(e^2)$
${}^1T_2(T_2) = -0.29\,{}^3T_1(et)-0.30\,{}^3T_1(t^2)+0.87\,{}^1T_2(et)-0.25\,{}^1T_2(t^2)$
${}^1A_1(A_1) = 0.11\,{}^3T_1(t^2)+0.90\,{}^1A_1(e^2)-0.41\,{}^1A_1(t^2)$
$b\,{}^3T_1(E) = -0.63\,{}^3T_1(et)+0.77\,{}^3T_1(t^2)$
$b\,{}^3T_1(T_2) = 0.58\,{}^3T_1(et)+0.69\,{}^3T_1(t^2)+0.42\,{}^1T_2(et)$
$b\,{}^3T_1(T_1) = -0.68\,{}^3T_1(et)+0.73\,{}^3T_1(t^2)$
$b\,{}^3T_1(A_1) = -0.69\,{}^3T_1(et)+0.72\,{}^3T_1(t^2)$

TABLE IV. The results of a two-photon intensity calculation are presented in the upper half of the table. The calculation, discussed in detail in the theory section, considers only the central metal ion in a cubic Coulomb field following the theory of Ref. 31. The lower part of the table presents a comparison of experimental and calculated relative two-photon intensities for the 0° and 45° spectra of the $^3T_2(T_1)$ state and between the $^3T_2(E)$ and $^3T_2(T_1)$ states at 45°.

Strong-field term	Substate	Intensity (0°)	Intensity (45°)	$\frac{I(45°)}{I(0°)}$
$^3T_2$	E	0	0.06	∞
	T_1	0.01	1.5	>100
	T_2	<0.01	0.14	>100
	A_2	0		n/a
^1E	E	0	20	∞
a^3T_1	A_1	0	17	∞
	T_1	0.9	68	79
	T_2	3.1	110	35
	E	0	61	∞
$^1T_2$	T_2	103	120	1.2
$^1A_1$	A_1	0	0.11	∞
b^3T_1	E	0	75	∞
	T_2	2.8	111	40
	T_1	1.2	69	55
	A_1	0	36	∞

Comparison between calculated and measured intensity ratios in the $^3T_2$ multiplet

	$\frac{I(T_1) \text{ at } 45°}{I(T_1) \text{ at } 0°}$	$\frac{I(T_1) \text{ at } 45°}{I(E) \text{ at } 45°}$
Experimental	3.0	1.1
Calculated	220	25

ization ratio of the $^1T_2$ state could not be measured this way, but based on signal-to-noise ratios and signal levels it probably ranges from 1 to 3.

Table IV clearly shows that there is a strong disagreement between the observed and calculated two-photon polarization ratios. The observed polarizations are much more isotropic than the calculated ones. The $^3A_2 \rightarrow {}^3T_2$ transition is forbidden without spin-orbit coupling so that only the small admixtures brought into the wave functions are important.

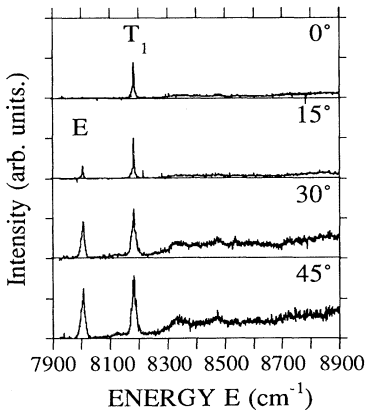

FIG. 11. Polarized two-photon spectra of the $^3A_2 \rightarrow {}^3T_2$ transition taken with a nonlinear reference. The relative intensity scales were obtained by fitting the intensities of the E-state zero-phonon lines to the symmetry-required $\sin^2 2\theta$ dependence.

Careful examination of the wave functions shows that the best way to introduce isotropic intensity (A_{1g} or E_g operators) into the two-photon transitions is to increase the fraction of the e^3t^5 configuration in the ground state. We tested the sensitivity of the wave function to changes in Dq, B, C, and ζ. The result was that the wave functions are very insensitive to the input parameters, even when the fit to the experimentally measured spectrum was quite poor. In fact, all attempts to modify the wave functions by individually changing Dq, B, C, and ζ failed to produce a significant change. This indicates that the crystal-field or d-electron approximation is inadequate to describe the $^3A_2 \rightarrow {}^3T_2$ two-photon transition. We note, however, that our calculations do give the correct ratio of $I(T_1)/I(E) \sim 1$ in the magnetic dipole spectrum of the $^3T_2$ state.

The d-electron approximation is adequate for the magnetic dipole spectrum because the angular momentum resides in the Ni^{2+} ion, but it is inadequate for two-photon electric dipole transitions, presumably because important contributions come from the ligands. Reid and Richardson[29] have shown that two-photon transitions in the rare earths in crystals may have dynamic contributions from the ligands which are comparable to those from the metal. It seems reasonable to suppose that in transition-metal systems the ligand contributions could be even greater because the radial wave functions of transition-metal ions extend farther from the center than in rare-earth ions. More systematic experimental and theoretical studies are needed to prove this.

The results for the allowed two-photon transitions do seem reasonable, however, and it is worthwhile to discuss them in detail. The relative intensities of the $a\ ^3T_1(T_1)$ and ^1E transitions are calculated to be about 3:1. The A_1 component is predicted to be much weaker than the other members of the multiplet because the minor contributions to the wave functions have the opposite sign from the $^3A_2(e^2)\rightarrow{}^3T_1(et)$ contribution. The $^1T_2$ state is surprisingly predicted to have the highest intensity of any of the ligand field transitions. It is difficult to prove this experimentally, especially without knowing the branching ratios for the luminescence to all the states of lower energy, since the two-photon excitation spectra were taken by monitoring the $^1T_2\rightarrow{}^3A_2$ emission. The predicted high intensity is the result of high-$^3T_1(et)$ character, the constructive addition of minor components, and the energy term in the denominator. The calculated polarization ratio of 1.2 appears to be close to the observed value. The $^1A_1$ state, on the other hand, has a very low intensity because it contains only a small contribution from the $^3T_1(et)$ basis state.

E. Assignments and dynamics of the ^1E and $a\ ^3T_1$ states

The ^1E line broadening must be related to rapid nonradiative decay into either the ground-state manifold or the $^3T_2$ state. The dominant channel has to be relaxation directly into the $^3T_2$ manifold since the excitation and absorption spectra are essentially identical as can be seen by comparing Fig. 9 to the absorption spectrum in Ref. 5. This is reasonable since the energy gap from the bottom of the ^1E surface to the E component of the $^3T_2$ multiplet is only 4500 cm^{-1}.

The large S factor in the ^1E state probably indicates a Jahn-Teller effect. This could be a combination of both first- and second-order contributions.[35] The first-order or in-state Jahn-Teller effect is possible since the state is doubly degenerate and both e_g and t_{2g} modes exist. Additionally, a second-order interaction with the $a\ ^3T_1(E)$ state, which lies at about 15 000 cm^{-1} a distance of 2500 cm^{-1} above the ^1E origin, is also possible. The eigenvectors derived from the full crystal-field calculations indicate that these two states are strongly mixed by spin-orbit coupling as shown in Table III.

The assignments of the $^3T_1$ spin-orbit components are problematic. In Payne's report[9] he assigns the 13 511-cm^{-1} feature as the $a\ ^3T_1(T_1)$ zero-phonon line based on direct observation in excited-state absorption at 95 K from the $^3T_2(E)$ state and also in luminescence from the $^1T_2$ state, which is vibronic so the local and lattice modes are seen. This is a reasonable assignment because the T_1 component is magnetic dipole allowed from the relaxed $^3T_2(E)$ state while the A_1 is not. The Franck-Condon center of the missing A_1 component of the $a\ ^3T_1$ state should lie near 13 838 cm^{-1} according to the calculation given in Table I, if the assignment of the 13 511-cm^{-1} line is accepted. Assuming the same S factor for it as for the other multiplet components, its zero-phonon line would be near 13 000 cm^{-1}. No feature in the 45° spectrum near this energy suggests such a line. If it is present, it is broadened beyond recognition.[36] It must also carry very little oscillator strength since the ^1E band in both one- and two-photon spectra is weak compared to the other multiplet components of $a\ ^3T_1$—note the relatively high oscillator strengths of the other multiplet components shown in Fig. 9, compared to that of the ^1E band. One possible reason for a broadening is that the zero-phonon line, as estimated from Table I, lies at the same energy as the band-mode sideband of the ^1E state. Vibrations of all symmetries occur at this energy, and would provide a way to couple ^1E and A_1 strongly. The calculated energies of the multiplet components of $a\ ^3T_1$ are in reasonable agreement with the present assignment.

V. CONCLUSIONS

In this study we have explored the application of single-beam two-photon excitation spectroscopy to Ni^{2+} in MgO. Our original goals of directly observing electronic origins and conclusively assigning the components in the three triplet multiplets have been partially realized. We have confirmed the symmetries of zero-phonon transitions in the $^3T_{2g}$, $^1T_{2g}$, and $b\ ^3T_{1g}$ states. Additionally, we now have a better understanding of the ion-lattice interaction through comparisons of one- and two-photon spectra.

We are able to explain why additional multiplet components do not appear in the $^3T_2$ two-photon spectra, but their absence from the $a\ ^3T_1$ and $b\ ^3T_1$ spectra is not understood. The $b\ ^3T_1(E)$ zero-phonon line has a width of 4-cm^{-1}, showing that it is not decaying on ultrafast time scales into the $^1T_2$ state. The T_2 component found in the 80-K double-excitation experiment[8] is no more broadened by the temperature than the E component; therefore, line broadening does not seem to explain the lack of intensity of the T_2 component, and by extension, that of the other two. Note, however, that the one-photon spectrum of the $b\ ^3T_1$ state, unlike the one-photon spectrum of the $a\ ^3T_1$ state, does not clearly show vibronic structure from more than the lowest-energy component.

Our two-photon relative intensity calculation appeared to work for the allowed two-photon transitions, but failed to describe adequately the intensities of the $^3A_2\rightarrow{}^3T_2$ transition. Our calculation dealt only with the d electrons of Ni^{2+} and there seems to be no way to calculate the right polarizations by changing the d-electron wave functions—within the constraint that the calculated energies still fit the experimental spectrum. This is possibly due to our neglect of ligand polarization contributions to the two-photon intensities as the O^{2-} ions in the coordination sphere of Ni^{2+} are highly polarizable, as shown by Reid and Richardson for rare earth ions.[29] Clearly, more sophisticated calculations such as those in Ref. 29 are needed to model the two-photon spectra in materials with highly polarizable ligands such as MgO:Ni^{2+}.

Another goal was to extend the technique of two-photon excitation further into the infrared where photomultipliers cannot be employed. This effort was partially successful. The power density in the sample was ~ 1 GW/cm^2 and although the crystal was not damaged

in a macroscopic sense, the spectra of the $^3T_2$ state degraded over time. We note that most other interesting inorganic impurity systems cannot withstand a power density of 1 GW/cm^2. Another limitation was that one-photon excited emission from centers other than octahedrally coordinated and isolated Ni^{2+} ions contaminated the two-photon spectra of the $a\ ^3T_1$ state. Typically in the visible and ultraviolet regions of the spectrum a gated boxcar integrator or interference filters could be used to isolate the desired emission. Unfortunately, most highly sensitive infrared detectors have slow response times, the selection of optical notch filters in the infrared is very poor, and, finally, in our two-photon excitation experiments, the signal to noise is already too low to withstand the losses inherent in using a monochromator.

Nevertheless, we have shown that two-photon spectroscopy can be performed on spectroscopic transitions as red as 1.2 μm. This technique can be applied to other impurity ions such as Co^{2+}, V^{2+}, and many rare earths: as long as the host medium can withstand the requiste high-power densities.

ACKNOWLEDGMENTS

We gratefully acknowledge the loan of MgO:Ni^{2+} crystals from Philip Stephens, Neil Manson, and Stephen Payne. We especially thank Stephen Payne and Richard Moncorgé for detailed discussions about the ^1E and $a\ ^3T_1$ states and Roberto Acevedo for assistance with the intensity calculation. Edward C. Lim, Edward I. Solomon, Neil Manson, Philip Stephens, and Colin Flint have also contributed with helpful discussions. Finally, we thank William Happer for loaning us his North Coast 77-K Ge photodiode. This work was supported by U.S. Department of Energy (DOE) Grant No. DE-FG02-84ER45146-A004 and the Exxon Research and Engineering Company.

[1]J. Ferguson, H. J. Guggenheim, and D. L. Wood, J. Chem. Phys. **40**, 822 (1964).
[2]J. Ferguson and H. J. Guggenheim, J. Chem. Phys. **44**, 1095 (1966).
[3]J. Ferguson, H. J. Guggenheim, H. Kamimura, and Y. Tanabe, J. Chem. Phys. **42**, 775 (1965).
[4]J. Ferguson, Aust. J. Chem. **21**, 323 (1968).
[5]B. D. Bird, G. A. Osborne, and P. J. Stephens, Phys. Rev. B **5**, 1800 (1972).
[6]N. B. Manson, Phys. Rev. B **4**, 2645 (1971).
[7]N. B. Manson, Phys. Rev. B **4**, 2656 (1971).
[8]R. Moncorgé and T. Benyattou, Phys. Rev. B **37**, 9186 (1988).
[9]S. A. Payne, Phys. Rev. B **41**, 6109 (1990).
[10]E. I. Solomon and C. J. Ballhausen, Mol. Phys. **29**, 279 (1975).
[11]W. E. Vehse, K. H. Lee, S. I. Yun, and W. A. Silbey, J. Lumin. **10**, 149 (1975).
[12]M. V. Iverson and W. A. Silbey, J. Lumin. **20**, 311 (1979).
[13]R. J. Tonucci, S. M. Jacobsen, and W. M. Yen, J. Lumin. **46**, 155 (1990).
[14]T. R. Bader and A. Gold, Phys. Rev. **171**, 997 (1968).
[15]P. Rabinowitz, B. N. Perry, and N. Levinos, IEEE J. Quantum Electron. **22**, 797 (1986).
[16]W. Low, Phys. Rev. **109**, 247 (1958).
[17]R. Pappalardo, D. L. Wood, and R. C. Linares, Jr., J. Chem. Phys. **35**, 1460 (1961).
[18]J. E. Ralph and M. G. Townsend, J. Phys. C **3**, 8 (1970).
[19]A. D. Liehr and C. J. Ballhausen, Ann. Phys. (N.Y.) **2**, 134 (1959).
[20]K. Y. Wong, D. Sengupta, and E. R. Krausz, Chem. Phys. Lett. **21**, 137 (1973).
[21]D. N. Copsey, A. J. McCafferty, R. Gale, M. D. Rowe, and P. Brint, Chem. Phys. Lett. **13**, 533 (1972).
[22]M. J. L. Sangster and C. W. McCombie, J. Phys. C **3**, 1498 (1970).
[23]C. K. Jorgensen, Acta. Chem. Scand. **9**, 1362 (1955).
[24]S. J. Mann and P. J. Stephens, Phys. Rev. B **9**, 863 (1974).
[25]A. Hjortsberg, J. T. Vallin, and F. S. Ham, Phys. Rev. B **37**, 3196 (1988).
[26]Neil Manson provided us with a crystal "grown from the melt in an electric arc furnace." The details are presented in his Ph.D. thesis, University of Aberdeen, 1968 (unpublished).
[27]B. R. Judd and D. R. Pooler, J. Phys. C **15**, 591 (1982).
[28]M. C. Downer, C. D. Cordero-Montalvo, and H. Crosswhite, Phys. Rev. B **28**, 4931 (1983).
[29]M. F. Reid and F. S. Richardson, Phys. Rev. B **29**, 2830 (1984).
[30]C. Campochiaro, D. S. McClure, P. Rabinowitz, and S. Dougal, Chem. Phys. Lett. **157**, 8 (1989).
[31]J. D. Axe, Jr., Phys. Rev. **136**, A42 (1964).
[32]J. S. Griffith, *The Theory of Transition Metal Ions* (Cambridge University Press, Cambridge, England, 1961).
[33]R. J. Powell and W. E. Spicer, Phys. Rev. B **2**, 2182 (1970).
[34]P. J. Stephens, (private communication).
[35]E. C. Lim, J. Phys. Chem. **90**, 6770 (1986).
[36]M. D. Sturge, H. J. Guggenheim, and M. H. L. Pryce, Phys. Rev. B **2**, 2459 (1970).